Food Science & Nutrition

WILEY

Food Science & Nutrition Open Access

ORIGINAL ARTICLE OPEN ACCESS

Atractylodes Macrocephala Polysaccharides Ameliorate Diabetic Hepatorenal Injury and Remodel Gut Microbiota in Mice

Jiali Wu[1] | Xuenan Liu[1] | Yangpeng Li[1] | Jing Liu[2] | Biao Jia[1] | Hongye Peng[3] | Qin Yuan[4] | Wen Liu[4] | Shengpeng Wang[4] | Duosheng Luo[1] | Xianglu Rong[1] | Wenliang Lv[2] | Jiao Guo[1]

[1]Guangdong Metabolic Diseases Research Center of Integrated Chinese and Western Medicine, Key Laboratory of Glucolipid Metabolic Disorder, Ministry of Education; Guangdong TCM Key Laboratory for Metabolic Diseases; Institute of Chinese Medicine, Guangdong Pharmaceutical University, Guangzhou, China | [2]Department of Infection, Guang'anmen Hospital, China Academy of Chinese Medical Sciences, Beijing, China | [3]Graduate School, Beijing University of Chinese Medicine, Beijing, China | [4]State Key Laboratory of Quality Research in Chinese Medicine, University of Macau, Macau, China

Correspondence: Wenliang Lv (lvwenliang@sohu.com) | Jiao Guo (gyguoyz@163.com)

Received: 19 January 2026 | **Revised:** 5 March 2026 | **Accepted:** 17 March 2026

Keywords: diabetes mellitus | diabetic kidney disease | gut microbiota | metabolome | nonalcoholic fatty liver disease | polysaccharides

ABSTRACT

Atractylodes macrocephala polysaccharides (AMPs) are known to exert metabolic regulatory and immunomodulatory activities, yet their protective effects across multiple organs in diabetes and the mechanisms involving gut-organ crosstalk have not been fully elucidated. In this study, we investigated the multi-organ benefits of AMPs in high-fat diet/streptozotocin-induced diabetic male C57BL/6 mice, with a particular focus on the gut microbiota-intestinal barrier-metabolite axis. Diabetic mice were treated with saline, losartan (30 mg/kg), metformin (100 mg/kg), or AMPs (100 or 300 mg/kg) for 8 weeks. Metabolic parameters, renal dysfunction, and hepatic injury were evaluated by measuring blood glucose, creatinine, proteinuria, and serum ALT/AST levels, together with histopathological examination. Inflammatory and fibrotic responses were assessed using qPCR, Western blotting, and immunostaining, while colonic barrier integrity was determined by the expression of the tight junction proteins ZO-1 and occludin. In addition, gut microbial composition was analyzed by 16S rRNA sequencing, and cecal metabolic profiles were characterized using LC–MS-based metabolomics. AMP treatment markedly improved glucose homeostasis and attenuated kidney and liver injury, as evidenced by reduced creatinine, proteinuria, ALT/AST levels, and tissue damage. These benefits were accompanied by decreased macrophage infiltration and suppression of inflammasome activation and fibrotic signaling. AMPs also alleviated colonic injury and restored intestinal barrier-associated proteins. Furthermore, AMP administration improved microbial diversity and altered the metabolic profile, with 134 differential metabolites identified, including several unsaturated

Abbreviations: α-SMA, alpha-smooth muscle actin; ALT, alanine aminotransferase; AMPK, AMP-activated protein kinase; AMPs, atractylodes macrocephala polysaccharides; AMPs-H, AMPs high dose; AMPs-L, AMPs low dose; Ara, arabinose; AST, aspartate aminotransferase; ATGL, Adipose triglyceride lipase; CD68, cluster of differentiation 68; CKD, chronic kidney disease; Cldn-2, claudin-2; Cldn-4, claudin-4; Col1a1, collagen type I alpha 1; CON, control; DKD, diabetic kidney disease; DM, diabetes mellitus; E-cadherin, epithelial cadherin; ESRD, end-stage renal disease; FN, fibronectin; FT-IR, Fourier-transform infrared spectroscopy; FTZ, Fufang Zhenzhu Tiaozhi; Gal, galactose; Gal UA, galacturonic acid; Glc, glucose; Glc UA, glucuronic acid; H&E, hematoxylin and eosin; HFD, high-fat diet; Il-1β, interleukin-1 beta; Il6, interleukin-6; KEGG, Kyoto encyclopedia of genes and genomes; LC–MS, Liquid chromatography–mass spectrometry; LEfSe, linear discriminant analysis effect size; LOS, losartan; LPS, lipopolysaccharide; MCP-1, monocyte chemoattractant protein-1; MET, metformin; NAFLD, non-alcoholic fatty liver disease; NF-κB, nuclear factor kappa-light-chain-enhancer of activated B cells; Nlrp3, NOD-LRR- and pyrin domain-containing protein 3; Ocln, occludin; OGTT, oral glucose tolerance test; OPLS-DA, orthogonal partial least squares discriminant analysis; PCoA, principal coordinates analysis; PPAR-γ, peroxisome proliferator-activated receptor gamma; SCFAs, short-chain fatty acids; SEM, scanning electron microscopy; Sob, species observed; SPF, specific pathogen-free; STZ, streptozotocin; T2DM, type 2 diabetes mellitus; TCM, traditional Chinese medicine; Tgfb1, transforming growth factor beta 1; Timp1, tissue inhibitor of metalloproteinases 1; TLR4, toll-like receptor 4; Tnfα, tumor necrosis factor alpha; UACR, urinary albumin-to-creatinine ratio; VIP, variable importance in projection; ZO-1, zonula occludens-1.

Jiali Wu, Xuenan Liu, and Yangpeng Li contributed equally to this work.

This is an open access article under the terms of the Creative Commons Attribution License, which permits use, distribution and reproduction in any medium, provided the original work is properly cited.

© 2026 The Author(s). *Food Science & Nutrition* published by Wiley Periodicals LLC.

fatty acids. Collectively, these findings suggest that AMPs protect the gut-liver-kidney axis, at least in part, by remodeling the gut microbiota, strengthening intestinal barrier function, and partially correcting disturbances in unsaturated fatty acid metabolism, highlighting their potential as an adjunctive therapeutic strategy for diabetic kidney disease and fatty liver disease.

1 | Introduction

Diabetes mellitus (DM) is a systemic metabolic disorder characterized by insulin resistance and chronic hyperglycemia (Xiong et al. 2023). Diabetic kidney disease (DKD) and nonalcoholic fatty liver disease (NAFLD) (Rivera-Esteban et al. 2023) frequently coexist with DM and markedly deteriorate the quality of life and prognosis of affected patients. Among these complications, DKD, a form of chronic kidney disease (CKD) secondary to DM, represents one of the principal microvascular complications of diabetes and is the leading cause of end-stage renal disease (ESRD) globally (Kim and Kim 2022). NAFLD is a metabolic disease driven by dysregulated glucose and lipid metabolism. NAFLD has a strong association with Type 2 diabetes mellitus (T2DM), as more than 90% of obese patients with T2DM also have NAFLD (Kumar et al. 2021). Pathologically, DKD is characterized by glomerular hyperfiltration, thickening of the glomerular basement membrane, inflammatory infiltration, and progressive renal fibrosis (Ricciardi and Gnudi 2021). Moreover, the pathogenesis of NAFLD primarily involves dysregulated lipid metabolism, dysfunction of the liver-pancreas axis, and persistent low-grade inflammation (Bedi et al. 2019). Despite affecting distinct organs, these diseases share considerable pathological overlap, including disturbances in glucose and lipid metabolism, insulin resistance, oxidative stress, chronic low-grade inflammation, and aberrant cytokine expression. This convergence of mechanisms provides a theoretical foundation for the development of integrated therapeutic strategies targeting both conditions simultaneously.

The intestinal microbiota is a complex ecosystem, and a growing body of evidence has revealed a strong association between the intestinal microbiota and various metabolic diseases such as diabetes, obesity, and cardiovascular disease (Gomes et al. 2018; Witkowski et al. 2020; Yang et al. 2021). Intestinal dysbiosis is primarily characterized by reduced microbial diversity and decreased abundance of both bacterial and fungal species (Jayasudha et al. 2020). Previous studies have shown that the gut microbiota interacts closely with the liver through the gut-liver axis, thereby affecting liver metabolism and immune function (Albillos et al. 2020). On one hand, gut microbes can regulate hepatic lipid metabolism by producing metabolites such as short-chain fatty acids (SCFAs), thereby preventing the development of hepatic steatosis (Li et al. 2023). On the other hand, microbial imbalance of the gut microbiota can trigger liver inflammation, increasing the susceptibility to liver diseases such as NAFLD, cirrhosis, and even hepatocellular carcinoma (Fang, Yu, et al. 2022; Liu and Yang 2023; Zhang et al. 2021). Disruption of the intestinal barrier may promote kidney disease and increase the risk of DKD (Lan et al. 2023). Most polysaccharides cannot be directly digested and absorbed by the human body. However, previous studies have shown that traditional Chinese medicine polysaccharides can influence the liver by modulating gut microbiota and its metabolic products (Fang, Wang, et al. 2022; Lan et al. 2024; Liu et al. 2024; Wu et al. 2025; Zhang et al. 2024).

Traditional Chinese medicine (TCM) polysaccharides are naturally occurring high-molecular-weight carbohydrates extracted from various parts of medicinal plants, including leaves, stems, flowers, fruits, and tubers (Liu and Huang 2019). Accumulating evidence suggests that TCM-derived polysaccharides may exert beneficial and preventive effects on diabetes-related complications, particularly DKD. For example, polysaccharides such as astragalus polysaccharide and Ganoderma lucidum polysaccharide have been reported to improve selected DKD-related indicators, including urinary protein excretion and renal function parameters (Chen et al. 2023; Guo et al. 2023; Pan et al. 2023; Zhang et al. 2007). Reported mechanisms include modulation of inflammatory responses, oxidative stress, immune regulation, and fibrosis-related processes. In addition, Banlanjian polysaccharides have been reported to improve serum lipid parameters (TC, TG, and LDL-C) in T2DM mice (Li et al. 2019).

Atractylodes macrocephala Koids. is a traditional Chinese medicinal and food-related plant with a long history of use in East Asia. AMPs are key bioactive polysaccharide constituents of *Atractylodes macrocephala* Koidz. Previous studies have reported multiple bioactivities of AMPs, including immunomodulatory, antioxidant, glycometabolic regulatory, and gastrointestinal protective effects (Feng et al. 2020; Guo et al. 2021; Kai et al. 2022; Luo et al. 2025; Xue et al. 2020; Zong et al. 2021). Evaluating the multi-organ protective associations of AMPs in diabetic liver and kidney injury, together with gut microbiota-related changes, may provide useful evidence for understanding their functional-food value and health-promoting potential in diabetes-associated complications.

The high-fat diet/streptozotocin (HFD/STZ)-induced diabetic mouse model was selected for its ability to reproduce key metabolic features of type 2 diabetes and its broad use in studies of diabetes-associated systemic complications. In this model, diabetic mice commonly develop hepatorenal injury together with gut microbiota dysbiosis and intestinal barrier impairment, which matches the pathological framework examined in this study. This model therefore serves as a practical platform for the simultaneous evaluation of liver and kidney injury and for the exploration of gut microbiota-related mechanisms associated with AMPs intervention. In this study, we evaluated the effects of AMPs on diabetic complications by measuring biochemical indicators and assessing histopathological changes in the liver and kidney tissues of HFD/STZ-induced DM mice. Furthermore, we explored potential regulatory mechanisms by examining its impact on gut microbiota and intestinal barrier function.

2 | Materials and Methods

2.1 | Materials and Reagents

STZ was obtained from Sigma Chemicals Co. Ltd. (St. Louis, USA). Creatinine and urine protein assay kits were procured from Nanjing Jiancheng Bioengineering Institute. The BCA Protein Assay Kit and DAB Substrate Kit were purchased from Thermo Fisher Scientific (Massachusetts, USA). The anti-GAPDH primary antibody was sourced from Beijing Zhongshan Golden Bridge Biotechnology Co. Ltd. (Beijing, China). The anti-FN and anti-TGF-β1 primary antibodies were acquired from Boster Biological Technology Co. Ltd. (California, USA), and the anti-Collagen-1 and anti-NLRP3 primary antibodies from Bioss (Boston, USA). The anti-CD68 primary antibody was obtained from Proteintech Group Inc. (Chicago, USA), and the anti-MCP-1 primary antibody from Santa Cruz Biotechnology Inc. (California, USA). The anti-ZO-1 and anti-Occludin primary antibodies were sourced from Abmart Pharmaceutical Technology Co. Ltd. (Shanghai, China). The Anti-Rabbit IgG (H + L) HRP Conjugate and Anti-Mouse IgG (H + L) HRP Conjugate were procured from Promega Co. Ltd. (Madison, Wisconsin, USA). Horseradish peroxidase-conjugated secondary antibody and antifade mounting medium were obtained from Beijing Zhongshan Golden Bridge Biotechnology Co. Ltd. (Beijing, China). Hematoxylin and eosin (H&E) staining solution, sodium dodecyl sulfate (SDS), acrylamide, loading buffer, and antifade mounting medium were purchased from Biosharp (Beijing, China). The Masson trichrome staining solution was procured from Leagene Biotech Co. Ltd. (Beijing, China). The SYBR Green Supermix was purchased from Bio-Rad Laboratories Inc. (California, USA). Isopropanol was obtained from Shanghai Macklin Biochemical Co. Ltd. (Shanghai, China). The reverse transcription kit was purchased from Takara Biotechnology Co. Ltd. (Dalian, China). Trizol was sourced from TransGen Biotech (Beijing, China).

2.2 | Preparation of AMPs

The Atractylodes macrocephala Koids. was purchased from Kangmei Pharmaceutical Co. Ltd. (Anhui, China). The characterization results of the AMPs, as previously reported in our earlier study (Wu et al. 2025), using ion chromatography (Dionex ICS-5000) for monosaccharide profiling, Fourier-transform infrared spectroscopy (FT-IR) for functional-group identification, and scanning electron microscopy (SEM) for microstructural observation, demonstrated that the primary monosaccharide component is glucan, with glucose (Glc) comprising 83.92% of the molecular weight. Other monosaccharides, including arabinose (Ara), galactose (Gal), galacturonic acid (Gal UA), and glucuronic acid (Glc UA), account for 7.19%, 5.47%, 3.00%, and 0.41%, respectively.

2.3 | Animals and Treatments

Male C57BL/6 mice (weighing 20 ± 2 g), aged 6 weeks, were provided by the Guangdong Provincial Medical Animal Center (Guangzhou, China, No. SCXK (YUE)2022-0002). All mice were housed in a sterile SPF environment, maintained on a 12-h light–dark cycle, at a temperature of 20°C–25°C and humidity of 60% ± 5%, with free access to water and food. All experimental procedures complied with Chinese animal welfare regulations and were approved by the Animal Ethics Committee of Guangdong Pharmaceutical University (Approval No. gdpulacspf2022097).

After a week of adaptive feeding, the mice were randomly divided into a control group and a high-fat diet (HFD) group. Based on references (Fan et al. 2018; Ji et al. 2016; Stephens and von der Weid 2020; Tahara and Takasu 2018), the model was established by feeding the high-fat diet group a high-fat diet (18% fat, 50% carbohydrates, and 19% protein) for 1 week, followed by intraperitoneal injections of STZ (50 mg/kg, dissolved in citrate buffer at pH 4.5) once daily for 5 consecutive days. One week after the final injection, fasting blood glucose levels were measured, and mice with values ≥ 16.7 mmol/L were considered diabetic and included in the study. These DM mice were then randomly divided into five groups ($n = 8$/group) and received daily gavage for 8 weeks: a DM model group (DM, saline), a losartan group (LOS, 30 mg/kg/day), a metformin group (MET, 100 mg/kg/day), a low-dose AMPs group (AMPs-L, 100 mg/kg/day), and a high-dose AMPs group (AMPs-H, 300 mg/kg/day). The control group (CON, saline) received saline gavage and citrate buffer injections, with regular feed. Body weight was monitored weekly for all mice. Each mouse was individually placed in metabolic cages for 24 h to collect urine samples. Following a 12-h fast and completion of the glucose tolerance test, mice were euthanized with a lethal dose of anesthetic. Blood, kidney, and intestinal tissue samples were collected immediately and stored at −80°C for subsequent analysis.

2.4 | Biochemical Assays

2.4.1 | Measurement of Fasting Blood Glucose

Random blood glucose levels were measured biweekly. In the eighth week after administration, fasting blood glucose levels were measured using a OneTouch Ultra blood glucose meter (Johnson & Johnson, USA).

2.4.2 | OGTT

The oral glucose tolerance test (OGTT) was used to assess glucose-induced changes in blood glucose levels. After an overnight fast (12 h), glucose (2 g/kg) was administered by gavage, and blood glucose levels were measured at 0, 15, 30, 60, 90, and 120 min post-administration (Wang et al. 2023).

2.4.3 | Biochemical Detection of Serum and Tissue Samples

Blood samples were centrifuged at 3000 rpm for 10 min to obtain the serum by extracting the supernatant. Urine samples were centrifuged at 3000 rpm for 5 min to remove sediment and obtain the urine samples. Blood creatinine and urine protein levels in mice were determined using creatinine assay kits and urine protein quantification kits.

2.4.4 | Histological Examinations

The collected kidney and colon tissues were soaked in fixative for 24 h, dehydrated, and then embedded in paraffin. The tissues were sectioned into 4 μm slices. Hematoxylin–eosin staining was employed to observe the tissue structure, and the slices were examined under a light microscope (Olympus, Tokyo, Japan). Masson's trichrome staining was utilized to evaluate the degree of renal fibrosis, and the blue fibrotic positive area was quantitatively analyzed using ImageJ software.

2.4.5 | Immunohistochemistry and Immunofluorescence Assay

Kidney sections were isolated and rehydrated, then incubated with anti-FN and anti-CD68 antibodies for immunohistochemical analysis. Colon sections were incubated with anti-ZO-1 antibodies followed by secondary antibody incubation, immunofluorescence staining, and image acquisition under a fluorescence microscope. The area of positive staining was measured and quantified using ImageJ software.

2.4.6 | Western Blot

Homogenize and centrifuge kidney/colon tissue to obtain total protein using RIPA lysis buffer containing 1% PMSF. Determine protein concentration with a BCA protein assay kit, separate using 10% SDS-PAGE, and transfer onto a polyvinylidene fluoride (PVDF) membrane. After blocking the membrane in TBST containing 5% non-fat milk for 1 h, incubate it with the primary antibody overnight at 4°C, followed by a 1-h incubation with an HRP-conjugated secondary antibody. Immerse in a well-mixed chemiluminescent developing solution and transfer to a chemiluminescence imaging system (Beijing Sage Creation Technology Co., China) for exposure and photography. Quantify band intensity using ImageJ software.

2.4.7 | Quantitative Real-Time Polymerase Chain Reaction

According to previous studies (Lan et al. 2023), total RNA was extracted from kidney or colon tissues treated with Trizol reagent, followed by reverse transcription and quantitative polymerase chain reaction. cDNA was synthesized from the extracted mRNA using Prime Script RT reagent with gDNA Eraser. Quantitative polymerase chain reaction was performed using SYBR Green SuperMix. Primer sequences for murine target genes, including Fn1, Ccl2, Il-1β, Nlrp3, Tgfb1, Zo-1, Ocln, Cldn-2, Cldn-4, Tlr-4, E-cadherin, Ppar-γ, Cd36, Il6, Tnfα, Col1a1, Timp1, Gapdh, and β-actin, were provided by Sangon Biotech (Shanghai) Co. Ltd. The relative abundance of each mRNA was calculated using the comparative threshold cycle (*C*t) method, with Gapdh or β-actin serving as reference genes. Primer sequences are provided in Table S1.

2.4.8 | 16S rRNA Gene Sequencing

Total genomic DNA from cecal contents was extracted using a DNA extraction kit. The quality of the extracted DNA was assessed using a Nanodrop micro-spectrophotometer (Thermo Fisher Scientific, USA) and agarose gel electrophoresis apparatus (LiuYi Instrument Factory, Beijing, China). The extracted genomic DNA was stored at −80°C for future use. The V3-V4 regions of bacterial 16S rRNA were amplified using forward primer 341F (5′-CCTACGGGNGGCWGCAG-3′) and reverse primer 806R (5′-GGACTACHVGGTWTCTAAT-3′), under the following conditions for the initial amplification: initial denaturation at 95°C for 5 min, followed by 30 cycles of denaturation at 95°C for 1 min, annealing at 60°C for 1 min, and extension at 72°C for 1 min, with a final extension at 72°C for 7 min. The PCR products were purified using AMPure XP Beads. The secondary amplification was carried out under the following conditions: initial denaturation at 95°C for 5 min, followed by 12 cycles of denaturation at 95°C for 1 min, annealing at 60°C for 1 min, and extension at 72°C for 1 min, with a final extension at 72°C for 7 min. The secondary amplification products were also purified using AMPure XP Beads. Subsequently, the amplified products were analyzed using the Illumina MiSeq platform (Illumina, SD, USA).

2.4.9 | UPLC-QTOF-MS-Based Metabolomics

After the sample of cecal contents is slowly thawed at 4°C, a suitable amount is mixed with a precooled methanol/acetonitrile/water solution (2:2:1, v/v) via vortexing to extract metabolites. Subsequently, the sample undergoes ultrasonic treatment at low temperature for 30 min, is allowed to stand at −20°C for 20 min, and then centrifuged at 4°C for 20 min. The supernatant is collected and dried under vacuum. The dried sample is then re-dissolved in a solvent containing 100 μL of acetonitrile/water (1:1, v/v), vortexed, and centrifuged at 4°C for 15 min. The supernatant is analyzed using an ultra-performance liquid chromatography (UPLC) system (Agilent, USA) coupled with a mass spectrometer (AB SCIEX, USA). The separation of the sample is performed on an Agilent 1290 Infinity LC UPLC HILIC column, with the column temperature set at 25°C, a flow rate of 0.5 mL/min, and an injection volume of 2 μL. The mobile phase A consists of water with 25 mM ammonium acetate and 25 mM ammonia, while mobile phase B is acetonitrile. The gradient elution program is as follows: from the initial time to 0.5 min, 95% B is maintained; from 0.5 to 7 min, B is linearly decreased to 65%; from 7 to 8 min, B is linearly decreased to 40%; from 8 to 9 min, B is held at 40%; from 9 to 9.1 min, B is linearly ramped up to 95%; and from 9.1 to 12 min, 95% B is maintained. During the analysis, the samples are kept in an autosampler at 4°C.

2.4.10 | Statistical Analysis

GraphPad Prism 9.2 was used to analyze the statistical significance of differences among groups. Differences between two groups were assessed using the unpaired *T*-test, and differences

among multiple groups were analyzed by one-way ANOVA. Data are expressed as mean ± SEM, and $p < 0.05$ was considered statistically significant.

3 | Results

3.1 | AMPs Improve Metabolic Control and Hepatic and Renal Function in Diabetic Mice

A diabetic mouse model was successfully established using a HFD/STZ administration (Figure 1A). AMPs significantly reduced fasting blood glucose, and the OGTT revealed that AMPs significantly enhanced insulin sensitivity in DM mice (Figure 1B,C). AMPs administration also led to marked reductions in serum creatinine, 24-h urinary protein excretion, and the urine albumin-to-creatinine ratio (UACR) (Figure 1D). In addition, AMPs significantly decreased serum levels of alanine aminotransferase (ALT) and aspartate aminotransferase (AST), indicating improved liver function (Figure 1E). Furthermore, H&E staining revealed glomerular hypertrophy in DM mice, which was alleviated by AMPs treatment (Figure 1F). Gross liver morphology and H&E staining showed that the AMPs treatment significantly reduced liver volume, hepatic lipid droplets, and alleviated hepatocyte necrosis, lipid vacuolization, and infiltration of inflammatory cells (Figure 1G). The data indicate that AMPs effectively ameliorated diabetes-induced liver and kidney dysfunction in mice.

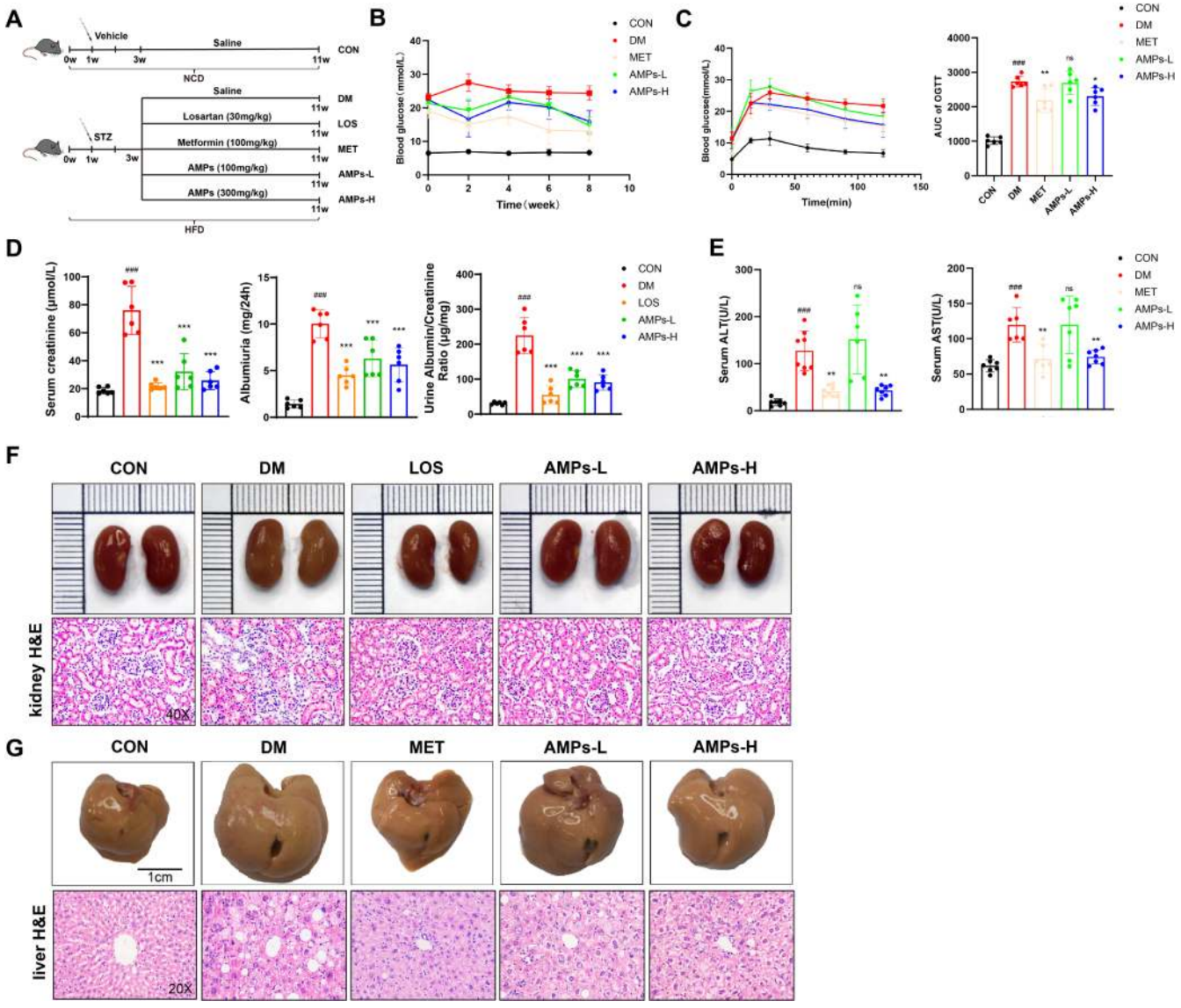


FIGURE 1 | Effects of AMPs on blood glucose, glucose tolerance, and hepatic and renal function in diabetic mice. (A) Schematic diagram of the experimental protocol; (B) Fasting blood glucose; (C) OGTT; (D) Serum creatinine content in each group of mice; 24-h urinary protein levels in each group of mice; urinary protein-to-creatinine ratio in each group of mice ($n = 6$); (E) ALT and AST; (F) Representative kidney appearance images and H&E staining of kidney tissue of mice in each group; (G) Gross liver morphology and HE staining. #indicates significant differences between the CON group and DM group; *indicates significant differences between AMPs-L/AMPs-H/LOS/MET groups and DM group. $^{\#\#\#}p < 0.001$, $^{*}p < 0.05$, $^{**}p < 0.01$, $^{***}p < 0.001$.

3.2 | AMPs Attenuate Renal Inflammation and Fibrosis in Diabetic Mice

To investigate the effects of AMPs on renal inflammation and fibrosis in diabetic mice, multiple histological and molecular analyses were performed. Immunohistochemical staining revealed a significant increase in CD68-positive macrophage infiltration in the kidneys of DM mice compared to controls, whereas treatment with losartan or AMPs markedly reduced CD68 expression, with the AMPs-H exhibiting the most pronounced effect (Figure 2A).

Consistently, quantitative PCR analysis demonstrated elevated mRNA expression of pro-inflammatory mediators *Ccl2*, *Il-1β*, and the inflammasome-related gene *Nlrp3* in the kidneys of diabetic mice. These increases were significantly suppressed following AMPs administration in a dose-dependent manner (Figure 2B). Western blot analysis further confirmed the reduction in NLRP3 and MCP-1 protein expression in the AMPs-treated groups, particularly in AMPs-H (Figure 2C).

Masson staining showed substantial renal interstitial collagen deposition in the DM group, indicative of fibrotic remodeling. This pathological alteration was significantly attenuated by AMPs treatment, as reflected by decreased collagen staining intensity (Figure 2D). Furthermore, immunohistochemical staining for fibronectin (FN) revealed marked accumulation of FN in the kidneys of diabetic mice, which was significantly reduced after both low- and high-dose AMPs intervention (Figure 2E).

At the transcriptional level, the expression of key fibrosis-related genes, including *Fn1*, *Col1a1*, and *Tgfb1*, was significantly upregulated in DM kidneys but was notably downregulated following AMPs treatment, as shown by qPCR (Figure 2F). These findings were corroborated by Western blot results, which demonstrated a similar trend at the protein level, with reduced expression of FN and collagen I after AMPs administration (Figure 2G).

Collectively, these results indicate that AMPs alleviate renal inflammation and fibrotic responses in diabetic mice, supporting their beneficial effects on kidney injury-related phenotypes in this model.

3.3 | AMPs Alleviate Hepatic Steatosis, Inflammation, and Fibrosis in Diabetic Mice

Oil Red O staining showed that AMPs treatment significantly reduced hepatic lipid droplets (Figure 3A). In addition, q-PCR analysis revealed that AMPs treatment significantly altered the mRNA expression of key hepatic lipid metabolism genes, specifically *Cd36* and *Ppar-γ* (Figure 3B). Protein level validation through Western Blot further confirmed the regulatory effect of AMPs treatment on the expression of PPAR-γ and ATGL, lipid metabolism-related proteins (Figure 3C).

CD68 immunohistochemical staining revealed extensive infiltration of macrophages surrounding the central veins and within the hepatic lobules in diabetic mice. This infiltration was markedly reduced in both AMPs-treated groups, with the high-dose group showing the most pronounced effect (Figure 3D). Further analysis through q-PCR revealed the effects of AMPs treatment on the expression of certain inflammation-related genes, including the hepatic mRNA levels of *Ccl2*, *Il6*, and *Tnf-α* (Figure 3E). Western blot analysis further confirmed the suppression of inflammation-related proteins, including NLRP3 and MCP-1, following AMPs administration (Figure 3F). Sirius Red staining of liver sections revealed that AMPs treatments significantly reduced the area of Sirius Red-positive regions in the liver (Figure 3G). mRNA levels of hepatic fibrosis-related genes *Tgfb1*, *Col1a1*, and *Timp1* were significantly decreased following AMPs treatments (Figure 3H). Western Blot analysis of hepatic fibrosis-related proteins showed a downward trend in the expression of Collagen-1 and α-SMA after AMPs intervention (Figure 3I). These results suggest that AMPs can attenuate hepatic lipid accumulation, inflammation, and fibrosis in DM mice.

3.4 | AMPs Restore Intestinal Mucosal Barrier Integrity and Reduce Colonic Inflammation in Diabetic Mice

Given that diabetes mellitus (DM) is frequently associated with intestinal barrier dysfunction (J. Zheng et al. 2018), the effects of AMPs on intestinal integrity were evaluated in the colons of diabetic mice. H&E staining of colon tissue samples showed (Figure 4A) that compared with the CON group, the crypts and goblet cells in the DM group were severely swollen and deformed, accompanied by inflammation. After 8 weeks of treatment with AMPs, crypt and goblet cell morphology improved and intestinal inflammation was reduced. The expression of ZO-1, a major component of intestinal tight junctions, was detected using immunofluorescence staining. As shown in Figure 4B, ZO-1 expression in the colon of DM mice was decreased but was significantly restored after AMPs treatment ($p < 0.001$). To further elucidate the molecular basis of this protective effect, the expression of tight junction-related genes was examined in colon tissue by quantitative PCR and Western blotting. As shown in Figure 4C, DM mice exhibited significant downregulation of *Zo-1*, *E-cadherin*, *Ocln*, *Cldn2*, and *Cldn4* mRNA expression compared with controls ($p < 0.001$), while AMPs treatment substantially reversed these changes. Similarly, Western Blot analysis showed (Figure 4D) that the protein expression levels of ZO-1 and Occludin were also significantly reduced. After treatment with AMPs (Figure S1), the protein expression levels of ZO-1 and Occludin increased ($p < 0.05$). Taken together, AMPs exhibit beneficial effects on intestinal integrity.

3.5 | AMPs Modulate Gut Microbiota Composition in Diabetic Mice

Gut microbiota composition was assessed by 16S rRNA sequencing at the experimental endpoint; therefore, the observed AMP-associated differences represent between-group compositional changes. 16S rRNA sequencing analysis was used to study the effect of AMPs on the intestinal flora of DM mice. Both Sob and Chao1 indices, which estimate microbial α-diversity, were significantly reduced in the DM group. In contrast, AMPs treatment restored these indices to levels comparable to the CON group (Figure 5A,B). PCoA analysis

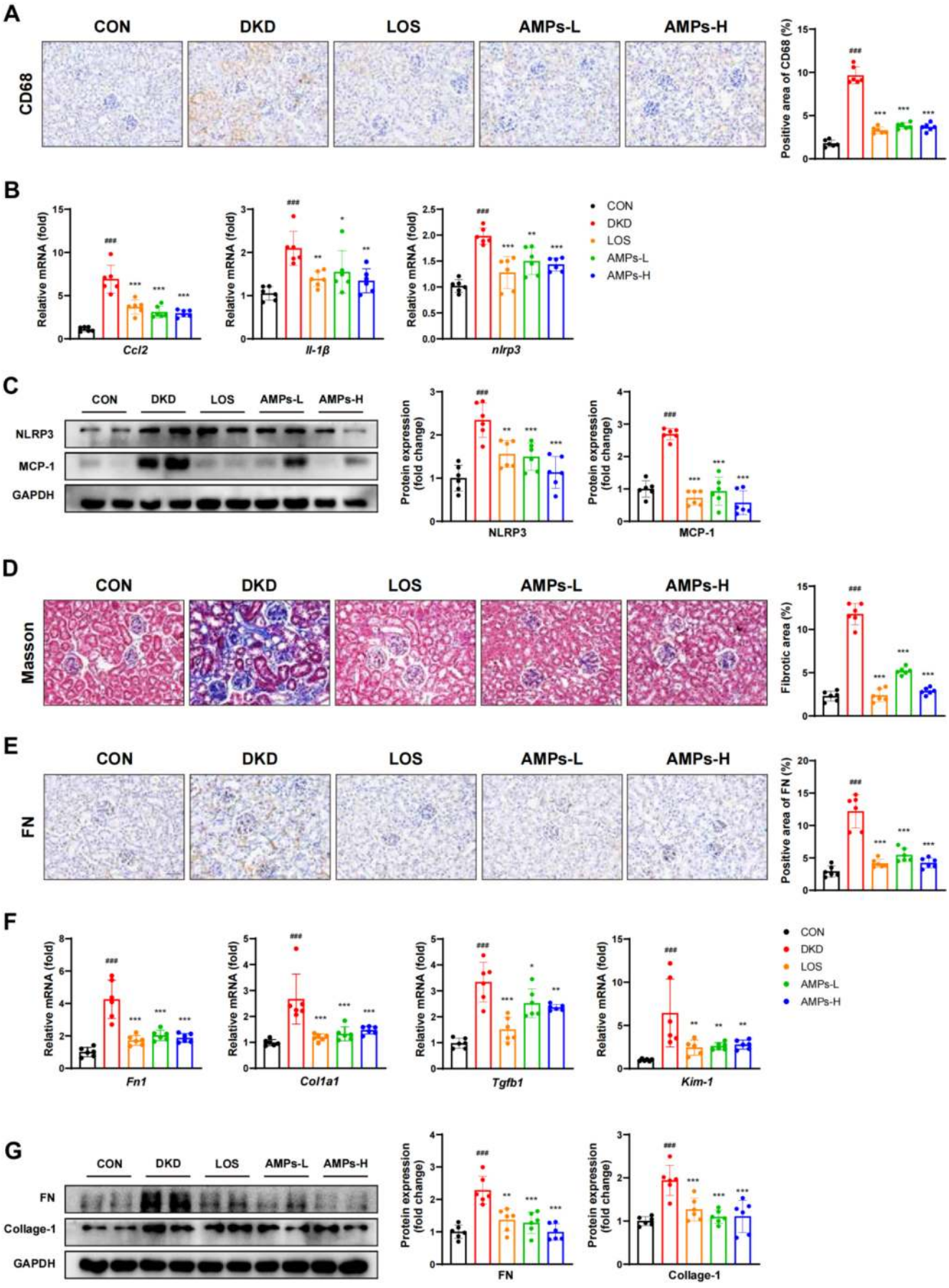


FIGURE 2 | Legend on next page.

FIGURE 2 | Renal histopathology and inflammatory and fibrotic markers in diabetic mice treated with AMPs. (A) Immunohistochemical staining and positive staining area of CD68 in mouse kidney, scale bar = 50 μm; (B) *q*-PCR was used to detect the mRNA expression of inflammatory factors *Ccl2*, *Il-1β*, and *Nlrp3* in the kidney; (C) Western blot was performed to detect the expression of MCP-1 and NLRP3 in the kidneys of DM mice, with GAPDH used as the internal reference for normalization; (D) Masson's trichrome staining of mouse kidney and positively stained areas, scale bar = 50 μm; (E) Immunohistochemical staining of FN in mouse kidney and FN-positive areas, scale bar = 50 μm; (F) *q*-PCR detection of mRNA expression of *Fn1*, *Col1a1*, and *Tgfb1* in the kidney; (G) Western blot analysis of FN and Collagen-1 expression in the kidneys of DM mice, with GAPDH as the internal reference for normalization ($n = 6$). #Indicates significant differences between the CON group and DM group; *indicates significant differences between AMPs-L/AMPs-H/LOS groups and DM group. $^{\#\#\#}p < 0.001$, $^{*}p < 0.05$, $^{**}p < 0.01$, $^{***}p < 0.001$.

showed clear separation among the CON, DM, and AMPs groups, with the AMPs group clustering closer to the CON group (Figure 5C). Taking phylum as the classification level, the stacked histogram of species composition revealed the distribution of intestinal microbiota, indicating that AMPs treatment helped restore the gut microbiota composition toward that of the CON group (Figure 5D). To identify differentially enriched bacterial taxa among the groups, linear discriminant analysis effect size (LEfSe) was performed. Distinct bacterial clades were identified as biomarkers for each group, indicating group-wise differences in gut microbial composition associated with AMPs treatment (Figure 5E).

LEfSe analysis identified distinct discriminative taxa across the CON, DM, and AMPs groups (Figure 5F). Notably, AMPs intervention reduced the relative abundance of *Desulfovibrionaceae* and increased several taxa enriched in the AMPs group, including *Clostridia*, *Lachnospiraceae NK4A136* group, and *Lactobacillus* (Figure 5G). Spearman correlation analysis further showed that taxa enriched after AMPs intervention were negatively correlated with renal injury-related indices, whereas Desulfovibrionaceae showed positive correlations (Figure 5H), suggesting an association between microbiota remodeling and improved renal outcomes.

3.6 | AMPs Alter Cecal Metabolite Profiles in Diabetic Mice

Untargeted metabolomics of cecal contents was performed to characterize AMP-associated metabolic shifts in diabetic mice. OPLS-DA showed a clear separation between the DM and AMPs groups, and the model validity was supported by permutation testing (Figure 6A,B). Differential metabolite screening based on VIP (≥ 1) and statistical significance identified a panel of metabolites altered between groups (Figure 6C).

Hierarchical clustering further revealed distinct group-wise metabolite patterns (Figure 6D). Differential metabolites include benzene and its derivatives, carboxylic acids and their derivatives, fatty acids, glycerophospholipids, imidazopyrimidines, indole and its derivatives, organic oxygen compounds, phenols, prenyl alcohol lipids, steroids and their derivatives, nucleosides and nucleotide analogs, etc. Among them, the content of benzene and its derivatives, carboxylic acids and their derivatives, fatty acids, and organic oxides is relatively low in DM mice; however, after AMPs treatment, the levels of these metabolites significantly increase.

3.7 | AMPs Modulate Cecal Metabolites Associated With Unsaturated Fatty Acid Metabolism in Diabetic Mice

Based on 16S rDNA sequencing data, PICRUSt analysis was used to infer microbial functional pathways potentially associated with AMPs treatment in diabetic mice, and 23 predicted metabolic pathways ($p < 0.01$) were identified (Figure 7A). In parallel, pathway enrichment analysis of differential metabolites was performed using the KEGG database. Based on criteria of pathway impact > 0.1 and $p < 0.05$, 11 significantly enriched metabolite-related pathways were identified (Figure 7B). By intersecting the predicted microbial pathways with the metabolite-enriched pathways, five shared pathways were obtained (Figure 7C), including biosynthesis of unsaturated fatty acids, glycerolipid metabolism, fatty acid biosynthesis, phenylalanine/tyrosine/tryptophan biosynthesis, and C5-branched dibasic acid metabolism. Among these, biosynthesis of unsaturated fatty acids was the top-ranked shared pathway.

Heatmap analysis suggested that AMPs treatment was associated with changes in several fatty acid metabolism-related pathways, including biosynthesis of unsaturated fatty acids (Figure 7D). Consistent with these pathway-level observations, representative unsaturated fatty acids (linoleic acid, α-linolenic acid, and oleic acid) were decreased in DM mice and partially restored after AMPs intervention (Figure 7E). Spearman correlation analysis indicated negative correlations between *Desulfovibrionaceae* and unsaturated fatty acid levels, whereas positive correlations were observed for *Clostridia*, *Lachnospiraceae NK4A136* group, and *Lactobacillus* (Figure 7F).

4 | Discussion

Atractylodes macrocephala, a classical herb with millennia of clinical use in traditional Chinese medicine, is a principal constituent of FTZ, Professor Jiao Guo's lipid-modulating formula developed according to the principle of "Tiao Gan Qi Shu Hua Zhuo" (soothing the liver, regulating spleen-Qi, and resolving turbidity). Our previous investigations demonstrated that FTZ ameliorates hepatic glucose–lipid metabolic disturbances and confers renoprotective effects in diabetic kidney disease (Lan et al. 2023; Lin et al. 2024; Wang et al. 2021). In this study, AMPs significantly ameliorated liver, kidney, and intestinal injury in HFD/STZ-induced diabetic mice. AMPs improved hepatic steatosis, inflammation, and fibrosis, while enhancing renal function, reducing glomerular hypertrophy, and suppressing pro-inflammatory and pro-fibrotic markers. Intestinal barrier

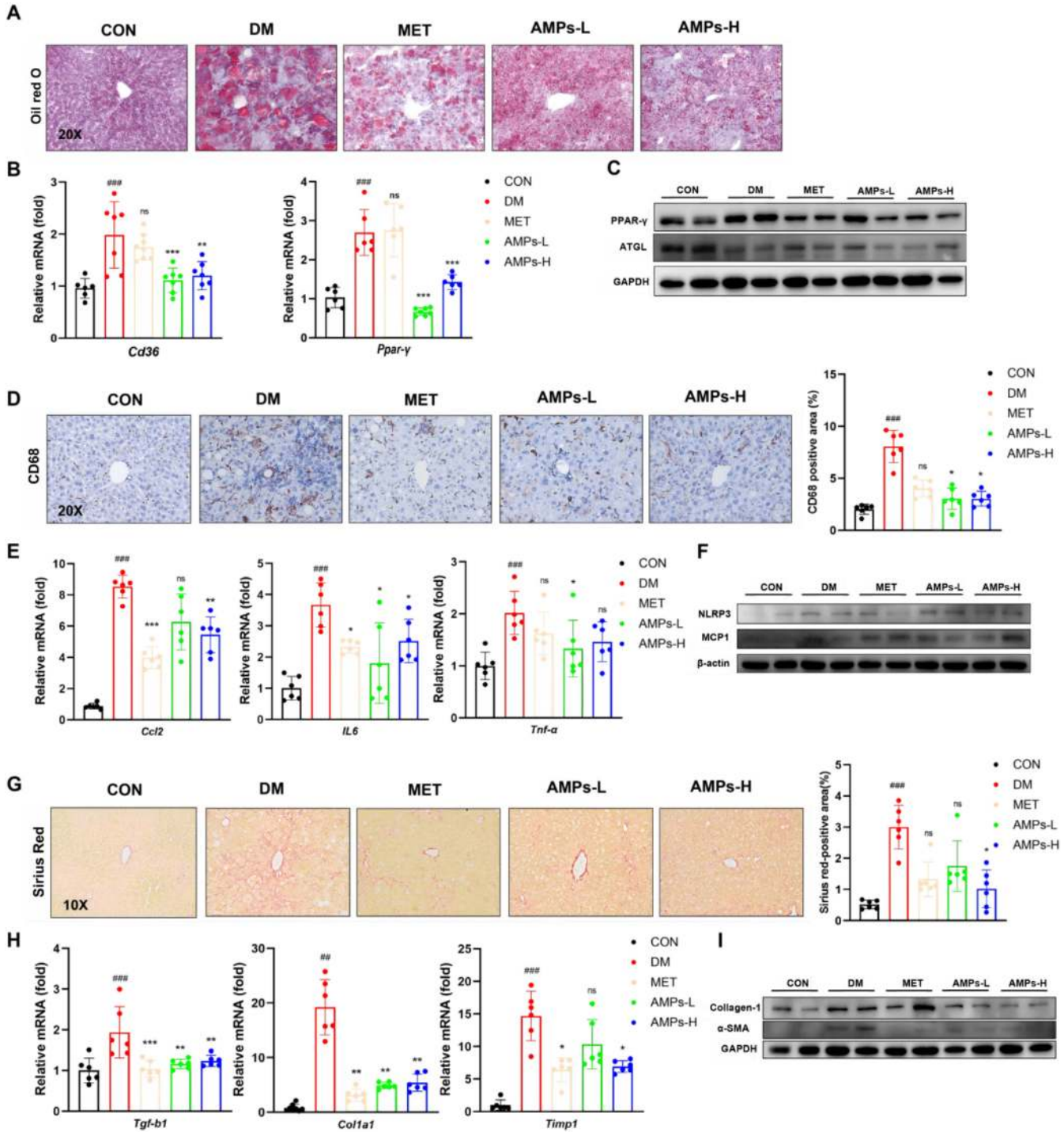


FIGURE 3 | Hepatic lipid accumulation, inflammatory infiltration, and fibrotic marker expression in diabetic mice after AMPs treatment. (A) Oil Red O staining; (B) *q*-PCR detection of mRNA expression of *CD36* and *Ppar-γ* in the liver; (C) Western blot was performed to detect the expression of PPAR-γ and ATGL in the liver, with GAPDH used as the internal reference for normalization; (D) Immunohistochemical staining and positive staining area of CD68 in liver; (E) *q*-PCR detection of mRNA expression of *Ccl2*, *IL6*, and *Tnf-α* in the liver; (F) Western blot was performed to detect the protein expression of NLRP3 and MCP-1 in the liver, with β-Actin used as the internal reference for normalization; (G) Sirius Red staining of liver sections and positively stained areas; (H) *q*-PCR detection of mRNA expression of *Tgf-b1*, *Col1a1*, and *Timp1* in the liver; (I) Western blot was performed to detect the expression of Collagen-1 and α-SMA in the liver, with GAPDH used as the internal reference for normalization. *Indicates significant differences between AMPs-L/AMPs-H/MET groups and DM group. $^{\#\#\#}p < 0.001$, $^{*}p < 0.05$, $^{**}p < 0.01$, $^{***}p < 0.001$.

integrity was restored through upregulation of tight-junction proteins (ZO-1, occludin) and attenuation of colonic inflammation. The combined 16S rDNA sequencing and metabolomics data support a potential contribution of gut microbiota remodeling to these multi-organ benefits. AMPs-treated mice showed enrichment of beneficial taxa (e.g., *Lachnospiraceae NK4A136 group* and *Lactobacillus*) and depletion of endotoxin-producing *Desulfovibrionaceae*, and these microbial shifts were

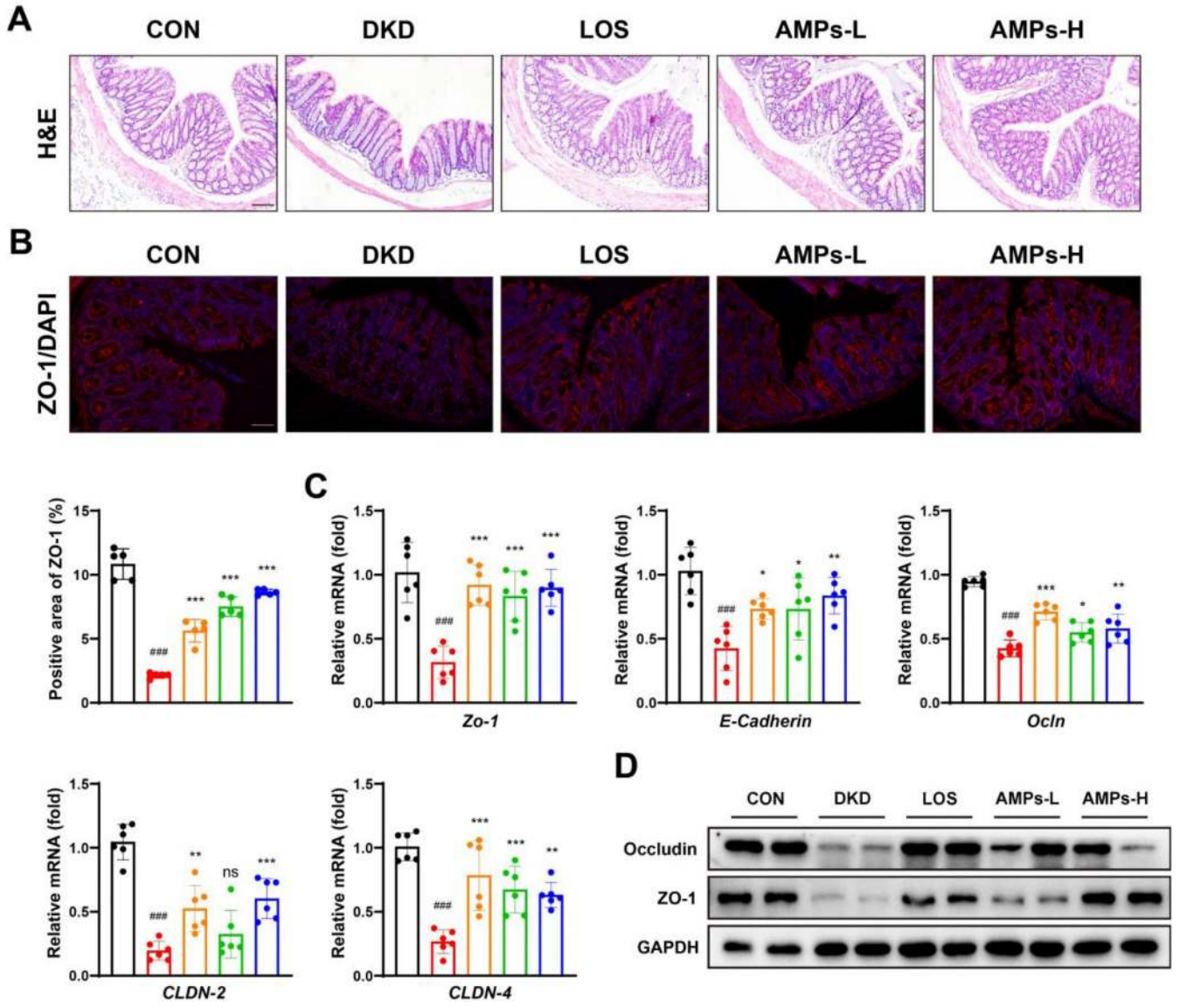


FIGURE 4 | Colonic histology and tight junction protein expression in diabetic mice treated with AMPs. (A) Colon tissue H&E staining, scale bar = 50 μm; (B) Immunofluorescence staining of ZO-1 (red) and ZO-1-positive area in colon tissue, scale bar = 50 μm; (C) q-PCR detection of mRNA expression of colonic tight junction proteins; (D) Protein expression levels of colonic tight junction proteins (ZO-1 and occludin), with GAPDH as the internal reference for normalization ($n = 6$). $^{\#}$Indicates significant differences between the CON group and DM group; *indicates significant differences between AMPs-L/AMPs-H/LOS groups and DM group. $^{\#\#\#}p < 0.001$, $^{*}p < 0.05$, $^{**}p < 0.01$, $^{***}p < 0.001$.

associated with predicted enrichment of pathways related to unsaturated fatty acid biosynthesis and with higher fecal levels of linoleic acid, α-linolenic acid, and oleic acid, correlating with improved lipid metabolism and reduced inflammation, particularly in the kidney. Collectively, these findings suggest that AMPs confer systemic protection in diabetic mice in association with gut microbiota compositional remodeling, metabolic changes, and reduced inflammatory burden along the gut-liver-kidney axis.

Rather than representing two independent sets of observations, the AMP-associated changes in gut microbiota and the improvements in liver and kidney injury may be interpreted within a linked gut-liver-kidney framework. In this study, AMP intervention was associated with partial restoration of microbial community structure, improved intestinal barrier-related markers, and altered cecal metabolite profiles, together with reduced inflammatory and oxidative stress indices and ameliorated hepatorenal injury. These findings support the possibility that gut microbiota remodeling acts as a potential mediating process through which AMP contributes to systemic protection in diabetic mice. A plausible interpretation is that AMP-associated microbiota modulation may help reduce intestinal dysfunction and metabolic disturbance, thereby lowering the translocation of pro-inflammatory signals and the systemic inflammatory burden, which in turn benefits both the liver and kidney. This integrative interpretation is consistent with the concurrent improvement in barrier integrity, inflammatory status, and tissue injury markers observed in our study. However, because this study was not designed to establish causality, these mechanistic links should be considered associative and hypothesis-generating, and they warrant further validation using microbiota-targeted causal approaches.

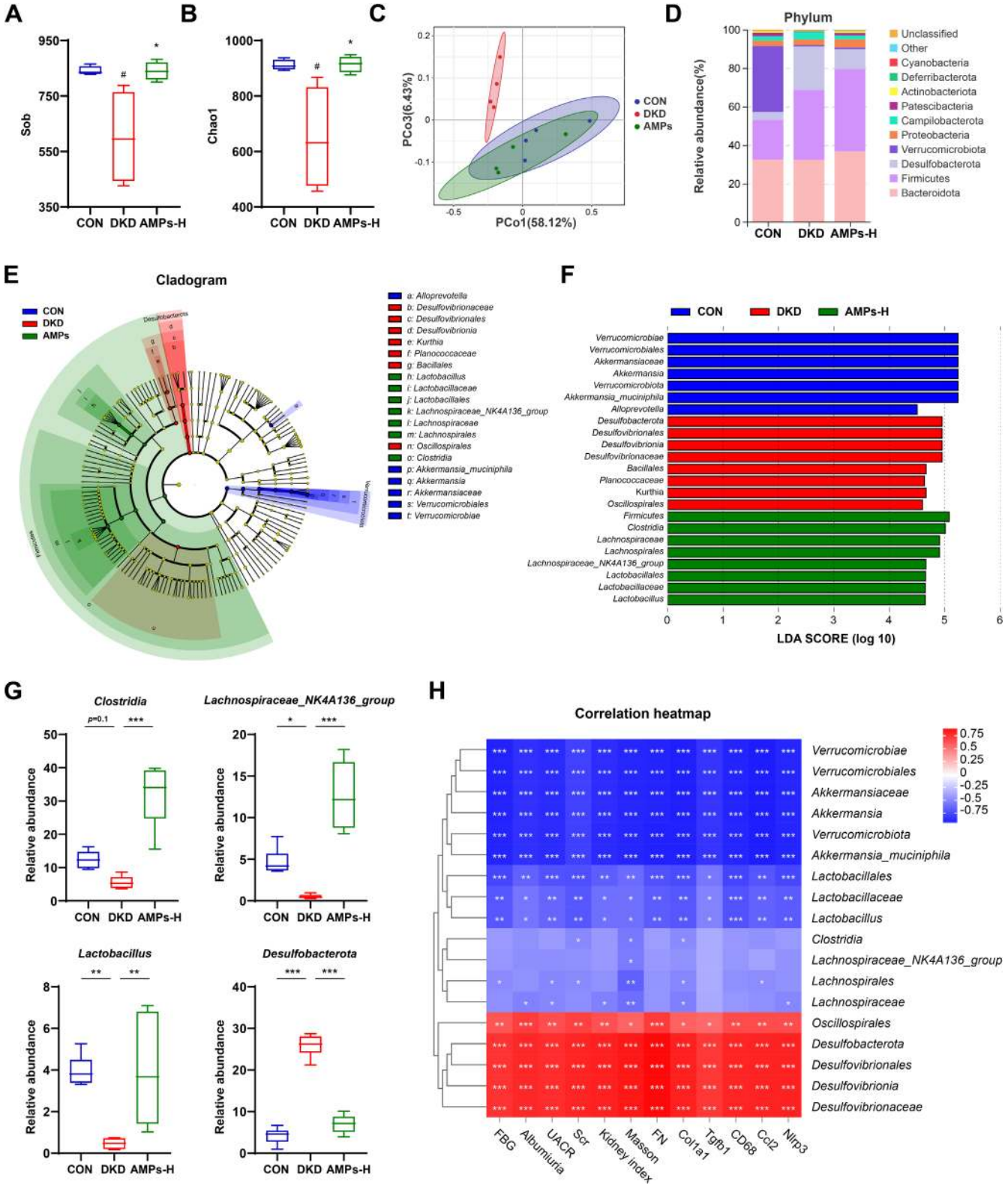


FIGURE 5 | Taxonomic composition and differential cecal bacterial genera in diabetic mice treated with AMPs. (A, B) Alpha diversity indices (Sob and Chao1) of each subgroup; (C) PCoA plot; (D) Stacked bar chart of species composition (at the phylum level); (E) Phylogenetic branch diagram with LDA score threshold set at 4.5, $n = 4$ per group; (F) LDA score plot; (G) Changes in relative abundance of *Clostridia*, *Lachnospiraceae_NK4A136_group*, *Lactobacillus*, and *Desulfovibrionaceae* after AMPs intervention; (H) Correlation analysis between DM-related biochemical indicators and gut microbiota. $^{\#}$indicates significant differences between the CON group and DM group; *indicates significant differences between AMPs-L/AMPs-H/LOS groups and DM group. $^{\#\#\#}p < 0.001$, $^{*}p < 0.05$, $^{**}p < 0.01$, $^{***}p < 0.001$.

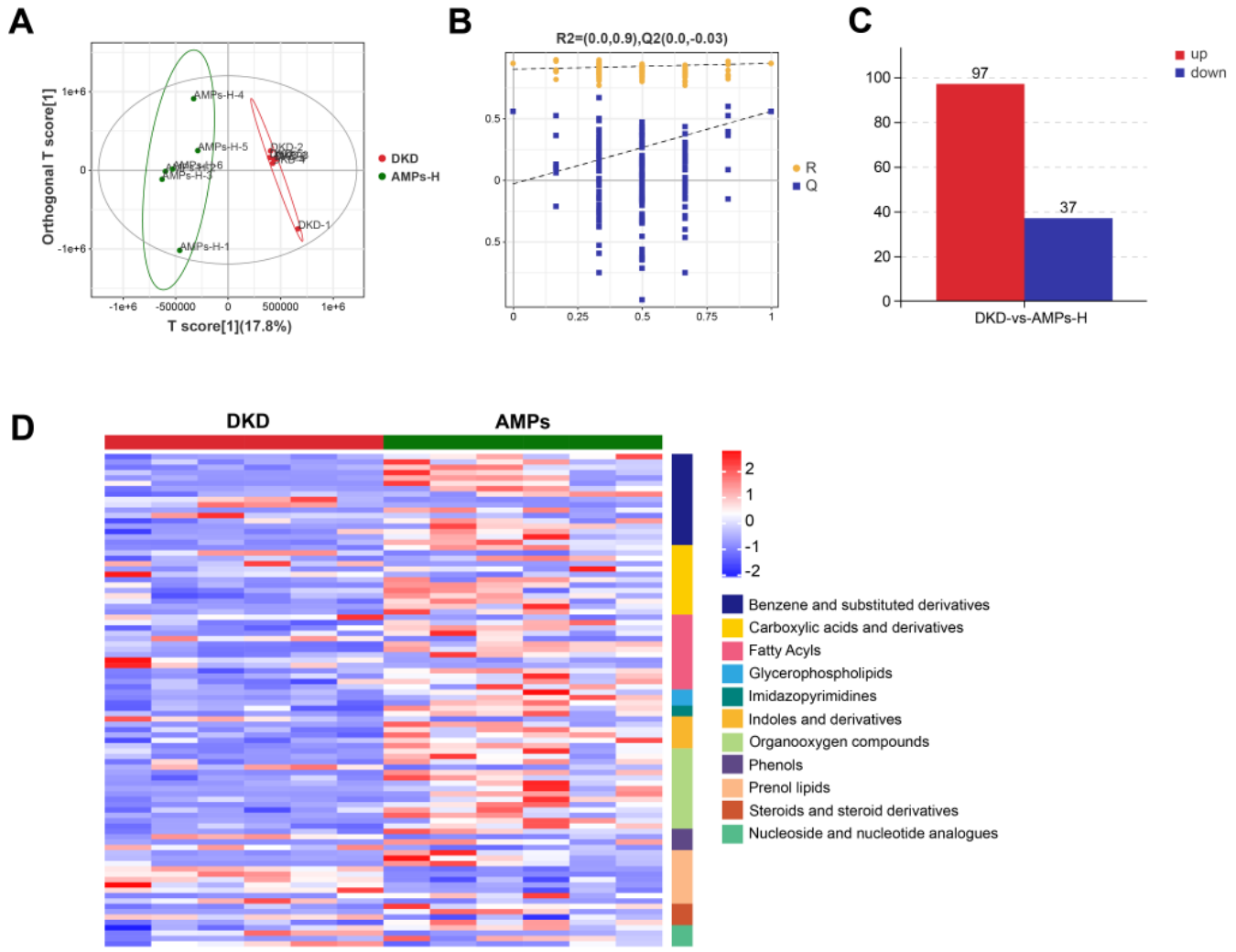


FIGURE 6 | Multivariate analysis and differential cecal metabolites in diabetic mice following AMPs treatment. (A, B) OPLS-DA results; (C) Differential metabolites between the DM group and AMPs group; (D) Heatmap of differential intestinal metabolites in mice following treatment with AMPs.

We purposefully selected two established positive controls to benchmark AMPs along organ-specific, pathophysiologic axes. Losartan (LOS) was chosen to evaluate renal efficacy in type 2 diabetic nephropathy: the RENAAL randomized trial demonstrated that LOS reduces proteinuria and slows progression to hard renal outcomes; mechanistically, RAAS blockade mitigates angiotensin II-driven TGF-β/Smad profibrotic signaling central to CKD fibrosis (Brenner et al. 2001; Li et al. 2024). Metformin (MET) was chosen to evaluate hepatic glucose-lipid metabolic efficacy: KDIGO 2022 endorses MET use in T2D with CKD when eGFR ≥ 30 mL/min/1.73 m^2, and mechanistic reviews support AMPK-dependent/independent actions that improve insulin resistance and hepatic glucose flux (Rena et al. 2017; Rinella et al. 2023).

Our findings align with prior evidence that Atractylodes macrocephala polysaccharides exert gut-protective and anti-inflammatory activities. In non-diabetic models, AMPs have been reported to modulate gut microbial dysbiosis, reduce pro-inflammatory cytokines, and enhance tight-junction protein expression, supporting improved barrier integrity (Kai et al. 2022). Consistent with these reports, AMPs intervention in diabetic mice was accompanied by reduced intestinal inflammation, improved barrier-related indices, and enrichment of beneficial genera such as Bifidobacterium and Lactobacillus, supporting a prebiotic-like role in shaping a healthier gut ecosystem. In diabetes, high-fat diets have been associated with expansion of LPS-related taxa such as Desulfovibrio and metabolic endotoxemia (Fuke et al. 2019) (Amar et al. 2011; Cani et al. 2007). The reduced abundance of Desulfovibrionaceae observed after AMPs intervention may therefore indicate a lower LPS-related inflammatory load, which is consistent with attenuated inflammatory mediators in hepatic and renal tissues and with a gut–organ inflammatory axis framework (Shi et al. 2006). Together, these findings support a microbiota–barrier–inflammation linkage through which AMPs may contribute to reduced TLR4/NF-κB–related inflammatory and fibrotic responses in diabetic liver and kidney injury.

Another key mechanism is the enhancement of unsaturated fatty acid metabolism associated with gut microbiota changes. AMPs increased the biosynthesis of linoleate, oleate, and other unsaturated fatty acids, which exert anti-inflammatory and organ-protective effects in diabetes. For example, oleic acid-rich diets

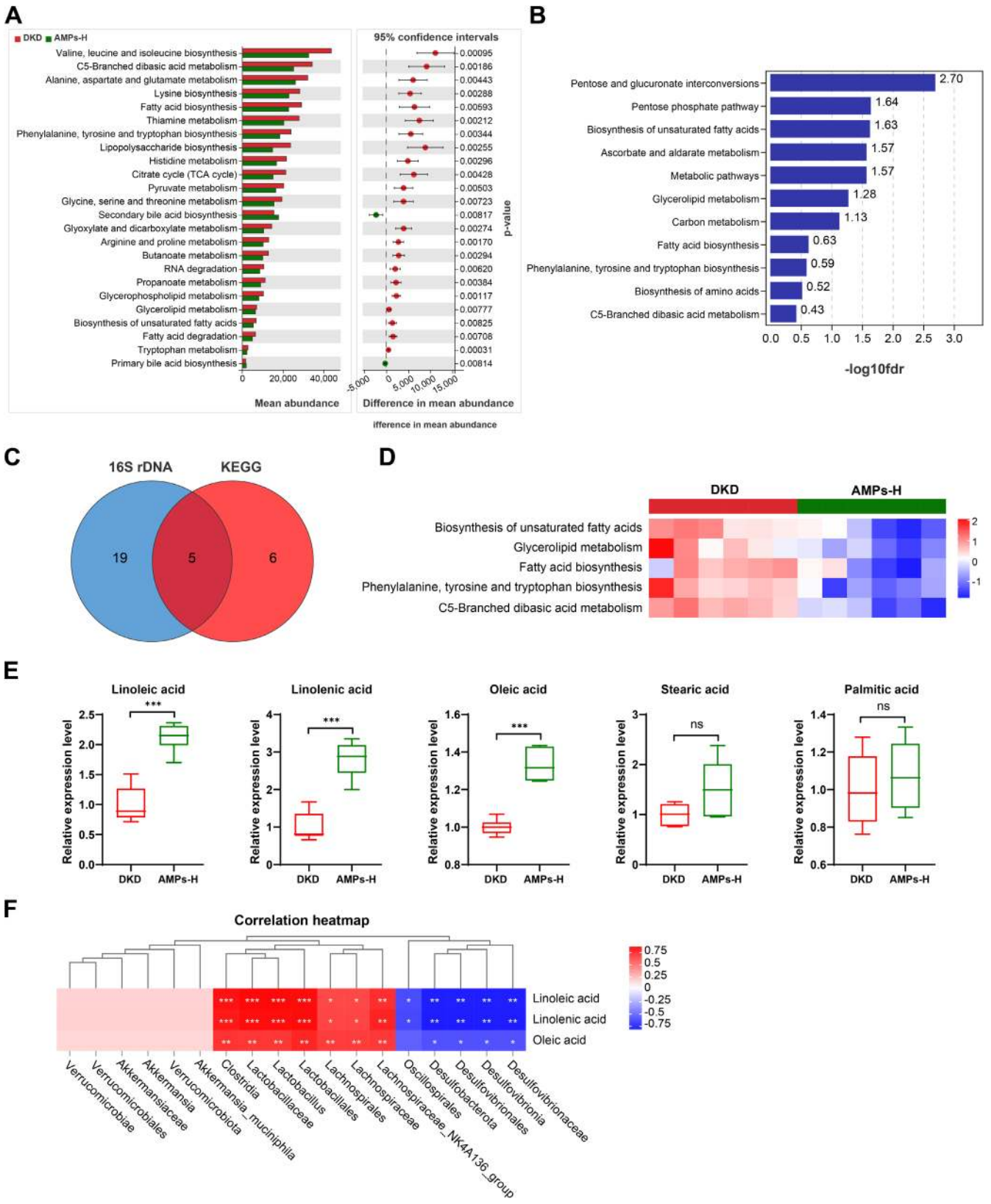


FIGURE 7 | Unsaturated fatty acid-related cecal metabolites and their correlations with gut microbiota and renal indices in diabetic mice treated with AMPs. (A) Analysis of differential metabolic pathways of intestinal flora in mice after AMPs treatment; (B) Pathway enrichment analysis of differential metabolites in mice after AMPs treatment; (C) Venn diagram; (D) Heatmap of co-occurring metabolic pathways between untargeted metabolomics and 16S rDNA sequencing; (E) Analysis of metabolites related to the biosynthesis of unsaturated fatty acids; (F) Spearman's correlation analysis. *Indicates significant differences between AMPs group and DM group, ***$p < 0.001$.

reduce lipotoxic kidney injury by alleviating ER stress (Pérez-Martí et al. 2022), and omega-3 fatty acids such as EPA and DHA are inversely associated with diabetic nephropathy and can inhibit renal fibrosis and inflammation (Xu et al. 2024). These changes may underlie the observed reductions in hepatic steatosis and renal inflammation. Moreover, certain *Lactobacillus* species produce conjugated linolenic acids and other fatty acid derivatives that improve glucose tolerance and suppress systemic inflammation (Festi et al. 2014; Lee et al. 2006; Putera et al. 2023). Thus, AMPs may act as prebiotic modulators, enriching beneficial microbes that generate favorable metabolites (SCFAs, conjugated fatty acids) while suppressing endotoxin producers, thereby restoring metabolic homeostasis and attenuating liver and kidney injury via the gut-liver-kidney axis.

AMPs may improve liver and kidney injury in diabetic mice not as two isolated outcomes, but through a shared gut-derived mechanism involving microbiota remodeling, intestinal barrier preservation, and metabolite rebalancing. Gut dysbiosis and barrier dysfunction are linked to systemic metabolic and inflammatory disturbances that can affect both hepatic and renal pathophysiology through gut–liver, gut–kidney, and broader gut–liver–kidney axis interactions (Dissayabutra et al. 2025; Fei et al. 2025; Pandey et al. 2025; Sokal-Dembowska et al. 2025). In MASLD-related settings, impaired intestinal permeability and translocation of microbial components have been associated with liver inflammation (Pandey et al. 2025; Sokal-Dembowska et al. 2025), whereas in DKD-related settings, gut dysbiosis, barrier impairment, endotoxin exposure, and metabolite imbalance have been linked to inflammatory and oxidative stress responses that contribute to kidney injury (Fei et al. 2025; Jiang et al. 2025; Zheng et al. 2025). In addition, comparative clinical data in MASLD and CKD indicate shared features of gut dysbiosis and intestinal barrier dysfunction, supporting the plausibility of partially convergent mechanisms across these organs (Dissayabutra et al. 2025). Therefore, the concurrent improvements in gut microbiota composition, intestinal barrier integrity, cecal metabolites, and liver/kidney injury markers observed after AMPs intervention may reflect a microbiota-associated reduction in systemic inflammatory-metabolic burden, rather than two unrelated parallel effects. However, this interpretation should be considered hypothesis-supportive rather than causal, and future studies using microbiota depletion, fecal microbiota transplantation, or targeted metabolite supplementation are needed to test mediation directly.

In summary, the present findings support a gut microbiota–associated systemic improvement framework in diabetic mice. AMPs intervention was accompanied by gut microbiota compositional remodeling, improved intestinal barrier-related indices, and rebalanced cecal metabolite profiles, together with attenuated inflammatory and oxidative stress markers and ameliorated liver and kidney injury. This integrative view helps unify the observed changes in inflammation, oxidative stress, and metabolic regulation as downstream manifestations of microbiota- and barrier-related modulation along a gut–liver–kidney interaction axis. Evidence in the current study remains associative rather than causal, and microbiota-depletion or fecal microbiota transplantation experiments, as well as targeted metabolite supplementation, will be valuable for testing mediation directly in future work.

5 | Conclusions

In summary, our study reveals the therapeutic effects and potential mechanisms of AMPs on diabetic liver and kidney damage in mice. AMPs can improve liver function and alleviate the relative liver weight in diabetic mice. Moreover, AMPs treatment significantly reduced liver volume and hepatic lipid droplets and alleviated hepatocyte necrosis, lipid vacuolization, and inflammatory cell infiltration. AMPs reduce the expression of genes associated with renal and colonic inflammatory responses, alleviating diabetic kidney damage induced by STZ combined with a high-fat diet. Furthermore, AMPs improve intestinal barrier function by restoring the expression of colonic tight junction proteins. Subsequent analysis of the gut microbiota and metabolites indicated that AMPs might ameliorate the dysregulated metabolism of unsaturated fatty acids in DM mice by increasing the abundance of *Clostridia*, *Lachnospiraceae NK4A136* group, and Lactobacillus in the cecum, while reducing the abundance of the harmful *Desulfovibrionaceae*. These findings support AMPs as a promising food-derived functional ingredient and microbiota-associated adjunctive strategy for improving diabetes-related liver and kidney injury in experimental settings.

Author Contributions

Jiali Wu: writing – original draft, writing – review and editing, visualization, investigation, data curation. **Xuenan Liu:** data curation, writing – original draft, writing – review and editing, investigation, visualization. **Yangpeng Li:** investigation, writing – original draft, writing – review and editing, visualization, data curation. **Jing Liu:** writing – review and editing, investigation, visualization, data curation, writing – original draft. **Biao Jia:** writing – review and editing, visualization, investigation, data curation. **Hongye Peng:** data curation, visualization, investigation. **Qin Yuan:** data curation. **Wen Liu:** data curation. **Shengpeng Wang:** data curation. **Duosheng Luo:** data curation. **Xianglu Rong:** data curation. **Wenliang Lv:** data curation. **Jiao Guo:** funding acquisition, conceptualization, project administration, data curation, supervision.

Acknowledgments

This work was supported by the National Key Research and Development Program of China (Grant No. 2023YFC3606200), National Natural Science Foundation of China (Grant No. T2341005), Department of Science and Technology of Guangdong Province (Grant No. 2019B030302005).

Funding

This work was funded by the National Key Research and Development Program of China (Grant No. 2023YFC3606200), National Natural Science Foundation of China (Grant No. T2341005), Department of Science and Technology of Guangdong Province (Grant No. 2019B030302005).

Conflicts of Interest

The authors declare no conflicts of interest.

Data Availability Statement

The data that support the findings of this study are available on request from the corresponding author. The data are not publicly available due to privacy or ethical restrictions.

References

Albillos, A., A. de Gottardi, and M. Rescigno. 2020. "The Gut-Liver Axis in Liver Disease: Pathophysiological Basis for Therapy." *Journal of Hepatology* 72, no. 3: 558–577. https://doi.org/10.1016/j.jhep.2019.10.003.

Amar, J., C. Chabo, A. Waget, et al. 2011. "Intestinal Mucosal Adherence and Translocation of Commensal Bacteria at the Early Onset of Type 2 Diabetes: Molecular Mechanisms and Probiotic Treatment." *EMBO Molecular Medicine* 3, no. 9: 559–572. https://doi.org/10.1002/emmm.201100159.

Bedi, O., S. Aggarwal, N. Trehanpati, G. Ramakrishna, and P. Krishan. 2019. "Molecular and Pathological Events Involved in the Pathogenesis of Diabetes-Associated Nonalcoholic Fatty Liver Disease." *Journal of Clinical and Experimental Hepatology* 9, no. 5: 607–618. https://doi.org/10.1016/j.jceh.2018.10.004.

Brenner, B. M., M. E. Cooper, D. de Zeeuw, et al. 2001. "Effects of Losartan on Renal and Cardiovascular Outcomes in Patients With Type 2 Diabetes and Nephropathy." *New England Journal of Medicine* 345, no. 12: 861–869. https://doi.org/10.1056/NEJMoa011161.

Cani, P. D., J. Amar, M. A. Iglesias, et al. 2007. "Metabolic Endotoxemia Initiates Obesity and Insulin Resistance." *Diabetes* 56, no. 7: 1761–1772. https://doi.org/10.2337/db06-1491.

Chen, Z., H. Liang, X. Yan, et al. 2023. "Astragalus Polysaccharide Promotes Autophagy and Alleviates Diabetic Nephropathy by Targeting the lncRNA Gm41268/PRLR Pathway." *Renal Failure* 45, no. 2: 2284211. https://doi.org/10.1080/0886022x.2023.2284211.

Dissayabutra, T., N. Chuaypen, P. Somnark, et al. 2025. "Characterization of Gut Dysbiosis and Intestinal Barrier Dysfunction in Patients With Metabolic Dysfunction-Associated Steatotic Liver Disease and Chronic Kidney Disease: A Comparative Study." *Scientific Reports* 15, no. 1: 15481. https://doi.org/10.1038/s41598-025-00237-6.

Fan, L., Q. Xiao, L. Zhang, et al. 2018. "CAPE-pNO(2) Attenuates Diabetic Cardiomyopathy Through the NOX4/NF-κB Pathway in STZ-Induced Diabetic Mice." *Biomedicine & Pharmacotherapy* 108: 1640–1650. https://doi.org/10.1016/j.biopha.2018.10.026.

Fang, J., C. H. Yu, X. J. Li, et al. 2022. "Gut Dysbiosis in Nonalcoholic Fatty Liver Disease: Pathogenesis, Diagnosis, and Therapeutic Implications." *Frontiers in Cellular and Infection Microbiology* 12: 997018. https://doi.org/10.3389/fcimb.2022.997018.

Fang, S., T. Wang, Y. Li, et al. 2022. "*Gardenia jasminoides* Ellis Polysaccharide Ameliorates Cholestatic Liver Injury by Alleviating Gut Microbiota Dysbiosis and Inhibiting the TLR4/NF-κB Signaling Pathway." *International Journal of Biological Macromolecules* 205: 23–36. https://doi.org/10.1016/j.ijbiomac.2022.02.056.

Fei, D. L., Y. Liu, J. Liu, Z. Yu, and J. L. Dong. 2025. "Gut Microbiota and the 'Gut-Liver-Kidney Axis' Theory: From Mechanisms to Therapeutics." *Frontiers in Microbiology* 16: 1554458. https://doi.org/10.3389/fmicb.2025.1554458.

Feng, W., J. Liu, Y. Tan, H. Ao, J. Wang, and C. Peng. 2020. "Polysaccharides From Atractylodes Macrocephala Koidz. Ameliorate Ulcerative Colitis via Extensive Modification of Gut Microbiota and Host Metabolism." *Food Research International* 138: 109777. https://doi.org/10.1016/j.foodres.2020.109777.

Festi, D., R. Schiumerini, L. H. Eusebi, G. Marasco, M. Taddia, and A. Colecchia. 2014. "Gut Microbiota and Metabolic Syndrome." *World Journal of Gastroenterology* 20, no. 43: 16079–16094. https://doi.org/10.3748/wjg.v20.i43.16079.

Fuke, N., N. Nagata, H. Suganuma, and T. Ota. 2019. "Regulation of Gut Microbiota and Metabolic Endotoxemia With Dietary Factors." *Nutrients* 11, no. 10: 2277. https://doi.org/10.3390/nu11102277.

Gomes, A. C., C. Hoffmann, and J. F. Mota. 2018. "The Human Gut Microbiota: Metabolism and Perspective in Obesity." *Gut Microbes* 9, no. 4: 308–325. https://doi.org/10.1080/19490976.2018.1465157.

Guo, M., J. Gao, L. Jiang, and Y. Dai. 2023. "Astragalus Polysaccharide Ameliorates Renal Inflammatory Responses in a Diabetic Nephropathy by Suppressing the TLR4/NF-κB Pathway." *Drug Design, Development and Therapy* 17: 2107–2118. https://doi.org/10.2147/dddt.S411211.

Guo, S., W. Li, F. Chen, et al. 2021. "Polysaccharide of Atractylodes Macrocephala Koidz Regulates LPS-Mediated Mouse Hepatitis Through the TLR4-MyD88-NFκB Signaling Pathway." *International Immunopharmacology* 98: 107692. https://doi.org/10.1016/j.intimp.2021.107692.

Jayasudha, R., T. Das, S. Kalyana Chakravarthy, et al. 2020. "Gut Mycobiomes Are Altered in People With Type 2 Diabetes Mellitus and Diabetic Retinopathy." *PLoS One* 15, no. 12: e0243077. https://doi.org/10.1371/journal.pone.0243077.

Ji, X., C. Li, Y. Ou, et al. 2016. "Andrographolide Ameliorates Diabetic Nephropathy by Attenuating Hyperglycemia-Mediated Renal Oxidative Stress and Inflammation via Akt/NF-κB Pathway." *Molecular and Cellular Endocrinology* 437: 268–279. https://doi.org/10.1016/j.mce.2016.06.029.

Jiang, H., X. Wang, W. Zhou, Z. Huang, and W. Zhang. 2025. "Gut Microbiota Dysbiosis in Diabetic Nephropathy: Mechanisms and Therapeutic Targeting via the Gut-Kidney Axis." *Frontiers in Endocrinology* 16: 1661037. https://doi.org/10.3389/fendo.2025.1661037.

Kai, L., X. Zong, Q. Jiang, et al. 2022. "Protective Effects of Polysaccharides From Atractylodes Macrocephalae Koidz. Against Dextran Sulfate Sodium Induced Intestinal Mucosal Injury on Mice." *International Journal of Biological Macromolecules* 195: 142–151. https://doi.org/10.1016/j.ijbiomac.2021.12.042.

Kim, M. K., and D. M. Kim. 2022. "Current Status of Diabetic Kidney Disease and Latest Trends in Management." *Journal of Diabetes Research* 13, no. 12: 1961–1962. https://doi.org/10.1111/jdi.13895.

Kumar, V., X. Xin, J. Ma, C. Tan, N. Osna, and R. I. Mahato. 2021. "Therapeutic Targets, Novel Drugs, and Delivery Systems for Diabetes Associated NAFLD and Liver Fibrosis." *Advanced Drug Delivery Reviews* 176: 113888. https://doi.org/10.1016/j.addr.2021.113888.

Lan, T., T. Tang, Y. Li, et al. 2023. "FTZ Polysaccharides Ameliorate Kidney Injury in Diabetic Mice by Regulating Gut-Kidney Axis." *Phytomedicine* 118: 154935. https://doi.org/10.1016/j.phymed.2023.154935.

Lan, T., J. Wu, B. Tang, et al. 2024. "Fufang Zhenzhu Tiaozhi Polysaccharides Ameliorates High-Fat Diet-Induced Non-Alcoholic Steatohepatitis and Intestinal Flora Disorders in Mice." *Journal of Functional Foods* 117: 106247.

Lee, H.-Y., J.-H. Park, S.-H. Seok, et al. 2006. "Human Originated Bacteria, *Lactobacillus rhamnosus* PL60, Produce Conjugated Linoleic Acid and Show Anti-Obesity Effects in Diet-Induced Obese Mice." *Biochimica et Biophysica Acta (BBA)-Molecular and Cell Biology of Lipids* 1761, no. 7: 736–744.

Li, J., Y. Zou, J. Kantapan, H. Su, L. Wang, and N. Dechsupa. 2024. "TGF-β/Smad Signaling in Chronic Kidney Disease: Exploring Post-Translational Regulatory Perspectives (Review)." *Molecular Medicine Reports* 30, no. 2: 143. https://doi.org/10.3892/mmr.2024.13267.

Li, J. P., Y. Yuan, W. Y. Zhang, et al. 2019. "Effect of Radix Isatidis Polysaccharide on Alleviating Insulin Resistance in Type 2 Diabetes Mellitus Cells and Rats." *Journal of Pharmacy and Pharmacology* 71, no. 2: 220–229. https://doi.org/10.1111/jphp.13023.

Li, Q., W. Liu, H. Zhang, et al. 2023. "α-D-1,3-Glucan From Radix Puerariae Thomsonii Improves NAFLD by Regulating the Intestinal Flora and Metabolites." *Carbohydrate Polymers* 299: 120197. https://doi.org/10.1016/j.carbpol.2022.120197.

Lin, Z., H. Huo, M. Huang, J. Tao, Y. Yang, and J. Guo. 2024. "Fufang Zhenzhu Tiaozhi (FTZ) Capsule Ameliorates Diabetic Kidney Disease in Mice via Inhibiting the SGLT2/Glycolysis Pathway." *Journal of Ethnopharmacology* 335: 118698. https://doi.org/10.1016/j.jep.2024.118698.

Liu, Q., Z. Zhang, P. Ji, et al. 2024. "Ginseng Polysaccharide Components Attenuate Obesity and Liver Lipid Accumulation by Regulating Fecal Microbiota and Hepatic Lysine Degradation." *International Journal of Biological Macromolecules* 269, no. 1: 131872. https://doi.org/10.1016/j.ijbiomac.2024.131872.

Liu, S., and X. Yang. 2023. "Intestinal Flora Plays a Role in the Progression of Hepatitis-Cirrhosis-Liver Cancer." *Frontiers in Cellular and Infection Microbiology* 13: 1140126. https://doi.org/10.3389/fcimb.2023.1140126.

Liu, Y., and G. Huang. 2019. "Extraction and Derivatisation of Active Polysaccharides." *Journal of Enzyme Inhibition and Medicinal Chemistry* 34, no. 1: 1690–1696. https://doi.org/10.1080/14756366.2019.1660654.

Luo, W., K. Zhang, Y. Wang, et al. 2025. "The Rhizome of Atractylodes Macrocephala Koidz.: A Comprehensive Review on the Traditional Uses, Phytochemistry and Pharmacology." *Chemistry & Biodiversity* 22, no. 3: e202401879. https://doi.org/10.1002/cbdv.202401879.

Pan, Y., Y. Zhang, J. Li, et al. 2023. "A Proteoglycan Isolated From Ganoderma Lucidum Attenuates Diabetic Kidney Disease by Inhibiting Oxidative Stress-Induced Renal Fibrosis Both In Vitro and In Vivo." *Journal of Ethnopharmacology* 310: 116405. https://doi.org/10.1016/j.jep.2023.116405.

Pandey, H., P. Goel, V. M. Srinivasan, D. W. T. Tang, S. H. Wong, and D. Lal. 2025. "Gut Microbiota in Non-Alcoholic Fatty Liver Disease: Pathophysiology, Diagnosis, and Therapeutics." *World Journal of Hepatology* 17, no. 6: 106849. https://doi.org/10.4254/wjh.v17.i6.106849.

Pérez-Martí, A., S. Ramakrishnan, J. Li, et al. 2022. "Reducing Lipid Bilayer Stress by Monounsaturated Fatty Acids Protects Renal Proximal Tubules in Diabetes." *eLife* 11: 74391. https://doi.org/10.7554/eLife.74391.

Putera, H. D., R. I. Doewes, M. N. Shalaby, et al. 2023. "The Effect of Conjugated Linoleic Acids on Inflammation, Oxidative Stress, Body Composition and Physical Performance: A Comprehensive Review of Putative Molecular Mechanisms." *Nutrition & Metabolism (London)* 20, no. 1: 35. https://doi.org/10.1186/s12986-023-00758-9.

Rena, G., D. G. Hardie, and E. R. Pearson. 2017. "The Mechanisms of Action of Metformin." *Diabetologia* 60, no. 9: 1577–1585. https://doi.org/10.1007/s00125-017-4342-z.

Ricciardi, C. A., and L. Gnudi. 2021. "Kidney Disease in Diabetes: From Mechanisms to Clinical Presentation and Treatment Strategies." *Metabolism* 124: 154890. https://doi.org/10.1016/j.metabol.2021.154890.

Rinella, M. E., B. A. Neuschwander-Tetri, M. S. Siddiqui, et al. 2023. "AASLD Practice Guidance on the Clinical Assessment and Management of Nonalcoholic Fatty Liver Disease." *Hepatology* 77, no. 5: 1797–1835. https://doi.org/10.1097/hep.0000000000000323.

Rivera-Esteban, J., M. Pons, A. Planas, et al. 2023. "Prediction of Clinical Events by Liver Stiffness and Chronic Kidney Disease by NAFLD in Patients With Type-2 Diabetes." *Gastroenterología y Hepatología* 46, no. 9: 682–691. https://doi.org/10.1016/j.gastrohep.2022.11.001.

Shi, H., M. V. Kokoeva, K. Inouye, I. Tzameli, H. Yin, and J. S. Flier. 2006. "TLR4 Links Innate Immunity and Fatty Acid-Induced Insulin Resistance." *Journal of Clinical Investigation* 116, no. 11: 3015–3025. https://doi.org/10.1172/jci28898.

Sokal-Dembowska, A., K. Ergan, and S. Jarmakiewicz-Czaja. 2025. "Role of Gut Microbiota in the Development of Metabolic Dysfunction-Associated Steatotic Liver Disease in Inflammatory Bowel Disease." *World Journal of Gastroenterology* 31, no. 40: 111375. https://doi.org/10.3748/wjg.v31.i40.111375.

Stephens, M., and P. Y. von der Weid. 2020. "Lipopolysaccharides Modulate Intestinal Epithelial Permeability and Inflammation in a Species-Specific Manner." *Gut Microbes* 11, no. 3: 421–432. https://doi.org/10.1080/19490976.2019.1629235.

Tahara, A., and T. Takasu. 2018. "Prevention of Progression of Diabetic Nephropathy by the SGLT2 Inhibitor Ipragliflozin in Uninephrectomized Type 2 Diabetic Mice." *European Journal of Pharmacology* 830: 68–75. https://doi.org/10.1016/j.ejphar.2018.04.024.

Wang, H., M. Huang, W. Bei, et al. 2021. "FTZ Attenuates Liver Steatosis and Fibrosis in the Minipigs With Type 2 Diabetes by Regulating the AMPK Signaling Pathway." *Biomedicine & Pharmacotherapy* 138: 111532. https://doi.org/10.1016/j.biopha.2021.111532.

Wang, W., M. Liang, L. Wang, W. Bei, and J. Guo. 2023. "15-Hydroxyprostaglandin Dehydrogenase Inhibitor SW033291 Ameliorates Hepatic Abnormal Lipid Metabolism, ER Stress, and Inflammation Through PGE(2)/EP4 in T2DM Mice." *Bioorganic Chemistry* 137: 106646. https://doi.org/10.1016/j.bioorg.2023.106646.

Witkowski, M., T. L. Weeks, and S. L. J. C. R. Hazen. 2020. "Gut Microbiota and Cardiovascular Disease." *Circulation Research* 127, no. 4: 553–570.

Wu, J., B. Jia, S. Gong, et al. 2025. "Protective Effects of Atractylodes Macrocephala Polysaccharides on Acetaminophen-Induced Liver Injury." *Frontiers in Pharmacology* 16: 1583334. https://doi.org/10.3389/fphar.2025.1583334.

Xiong, P., F. Zhang, F. Liu, et al. 2023. "Metaflammation in Glucolipid Metabolic Disorders: Pathogenesis and Treatment." *Biomedicine & Pharmacotherapy* 161: 114545. https://doi.org/10.1016/j.biopha.2023.114545.

Xu, S., X. Li, Q. Hou, et al. 2024. "Association of Serum Unsaturated Fatty Acid Patterns With the Risk of Diabetic Nephropathy." *Kidney Diseases* 10, no. 2: 97–106. https://doi.org/10.1159/000536532.

Xue, W., Y. Gao, Q. Li, et al. 2020. "Immunomodulatory Activity-Guided Isolation and Characterization of a Novel Polysaccharide From Atractylodis Macrocephalae Koidz." *International Journal of Biological Macromolecules* 161: 514–524. https://doi.org/10.1016/j.ijbiomac.2020.06.003.

Yang, G., J. Wei, P. Liu, et al. 2021. "Role of the Gut Microbiota in Type 2 Diabetes and Related Diseases." *Metabolism* 117: 154712. https://doi.org/10.1016/j.metabol.2021.154712.

Zhang, L., Y. Liu, Q. Zhang, et al. 2024. "*Salvia miltiorrhiza* Polysaccharide Mitigates AFB1-Induced Liver Injury in Rabbits." *Ecotoxicology and Environmental Safety* 276: 116344. https://doi.org/10.1016/j.ecoenv.2024.116344.

Zhang, X., O. O. Coker, E. S. Chu, et al. 2021. "Dietary Cholesterol Drives Fatty Liver-Associated Liver Cancer by Modulating Gut Microbiota and Metabolites." *Gut* 70, no. 4: 761–774. https://doi.org/10.1136/gutjnl-2019-319664.

Zhang, Y. W., C. Y. Wu, and J. T. Cheng. 2007. "Merit of Astragalus Polysaccharide in the Improvement of Early Diabetic Nephropathy With an Effect on mRNA Expressions of NF-kappaB and IkappaB in Renal Cortex of Streptozotoxin-Induced Diabetic Rats." *Journal of Ethnopharmacology* 114, no. 3: 387–392. https://doi.org/10.1016/j.jep.2007.08.024.

Zheng, J., X. Yuan, G. Cheng, et al. 2018. "Chitosan Oligosaccharides Improve the Disturbance in Glucose Metabolism and Reverse the Dysbiosis of Gut Microbiota in Diabetic Mice." *Carbohydrate Polymers* 190: 77–86. https://doi.org/10.1016/j.carbpol.2018.02.058.

Zheng, X., X. Luo, Y. Zhang, et al. 2025. "Inflammation in Diabetic Kidney Disease Is Linked to Gut Dysbiosis and Metabolite Imbalance." *Journal of Diabetes* 17, no. 12: e70175. https://doi.org/10.1111/1753-0407.70175.

Zong, X., X. Xiao, L. Kai, et al. 2021. "Atractylodis Macrocephalae Polysaccharides Protect Against DSS-Induced Intestinal Injury Through a Novel lncRNA ITSN1-OT1." *International Journal of Biological Macromolecules* 167: 76–84. https://doi.org/10.1016/j.ijbiomac.2020.11.144.

Supporting Information

Additional supporting information can be found online in the Supporting Information section. **Appendix S1:** fsn371700-sup-0001-AppendixS1.docx.